Radiat Med (2008) 26:70–75
DOI 10.1007/s11604-007-0197-4

ORIGINAL ARTICLE

Percutaneous vertebroplasty performed by the isocenter puncture method

Shinjirou Sakaino · Kenji Takizawa
Misako Yoshimatsu · Yukihisa Ogawa
Kunihiro Yagihashi · Yasuo Nakajima

Received: July 17, 2007 / Accepted: October 9, 2007

Abstract
Purpose. The aim of this study was to clarify the usefulness of the isocenter puncture (ISOP) method.
Materials and methods. We investigated 73 vertebral bodies that had undergone percutaneous vertebroplasty (PVP) by the ISOP method, 118 vertebral bodies that had undergone the puncture simulation method, and 33 vertebral bodies that had undergone the conventional method. The items to be examined included the success rate (SR) of the median puncture of the vertebral body and the procedure time. The puncture accuracy and fluoroscopy time were also measured for the ISOP method.
Results. The SR was significantly higher and the procedure time significantly shorter when using the ISOP method rather than the conventional method. However, no significant differences were observed between the ISOP method and the puncture simulation method. The errors between the puncture needle tip and the puncture target point in the ISOP method were an average of 1.52, 2.08, and 1.87 mm in each of the horizontal, ventrodorsal, and craniocaudal directions. The fluoroscopy time when operating on one vertebral body was an average of 5.8 min.
Conclusion. The ISOP method is considered to be a useful approach while also reducing the puncture time and the fluoroscopy time.

S. Sakaino (✉) · K. Takizawa · M. Yoshimatsu · Y. Ogawa · K. Yagihashi · Y. Nakajima
Department of Radiology, St. Marianna University School of Medicine, 2-16-1 Sugao, Miyamae, Kawasaki 216-8511, Japan
Tel. +81-44-977-8111; Fax +81-44-589-9797
e-mail: sakashin622@yahoo.co.jp

This article was presented at a Japan Radiological Society meeting in April 2007

Key words ISOP method · Percutaneous vertebroplasty · Unilateral transpedicular approach Isocenter marker · PVP

Introduction

Percutaneous vertebroplasty (PVP), a rapidly acting treatment for pain caused by a compressed fracture of the vertebral body, is increasingly being used worldwide. PVP is generally performed using a C-arm radiographic system and puncturing the vertebral arch pedicle percutaneously under X-ray fluoroscopy. The puncture approach includes both the unilateral and bilateral transpedicular approaches. The unilateral transpedicular approach is relatively difficult to perform as it requires advancing the tip of a puncture needle to the midline of the vertebral body. Therefore, some institutions use the bilateral transpedicular approach. However, the unilateral transpedicular approach may decrease the number of punctures required during such surgery.[1,2]

We have therefore developed an isocenter puncture (ISOP) method[3], which is a puncture support method for the unilateral transpedicular approach. The ISOP method allows pinpoint targeting and puncturing of a target within the vertebral body under X-ray fluoroscopy.

We herein describe the results of PVP using the ISOP method and compare the findings with those achieved with the puncture simulation method[2] using the puncture angle measured by the preoperative CT examination and those by the conventional puncture method, as a historical control, while also examining the usefulness of the ISOP method.

Materials and methods

This study was approved by the ethics committee at our institution.

ISOP method concept and procedures

The isocenter of the C-arm radiographic system is the center of the radiation field and the center of the C-arm rotation. Therefore, regardless of how the C-arm rotates, the isocenter always remains at the center of the radiation field and the center of the monitor screen. The ISOP method applies this principle, and therefore adjusting the puncture target to the position of the isocenter becomes essential with this method. For this purpose, we created a black dot-like isocenter marker (ICM; Toshiba Medical, Tokyo, Japan), which is constantly illuminated at the center of the fluoroscopic monitor screen (Fig. 1).[2] We set the anterior one-third median site of the vertebral body as a target point.

The procedures of the ISOP method start with positioning the puncture target point at the isocenter. The first step is a frontal view on the fluoroscopic monitor. The examining table is moved as necessary to align it with the median of the vertebral body with the ICM (Fig. 2a). Next, the lateral view is used with the C-arm tilted 90° for guidance. The examining table is moved so that the anterior one-third median site of the vertebral

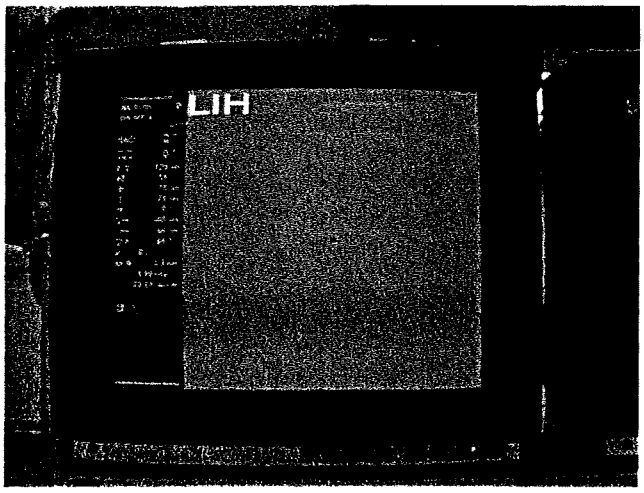

Fig. 1. Isocenter marker (ICM)

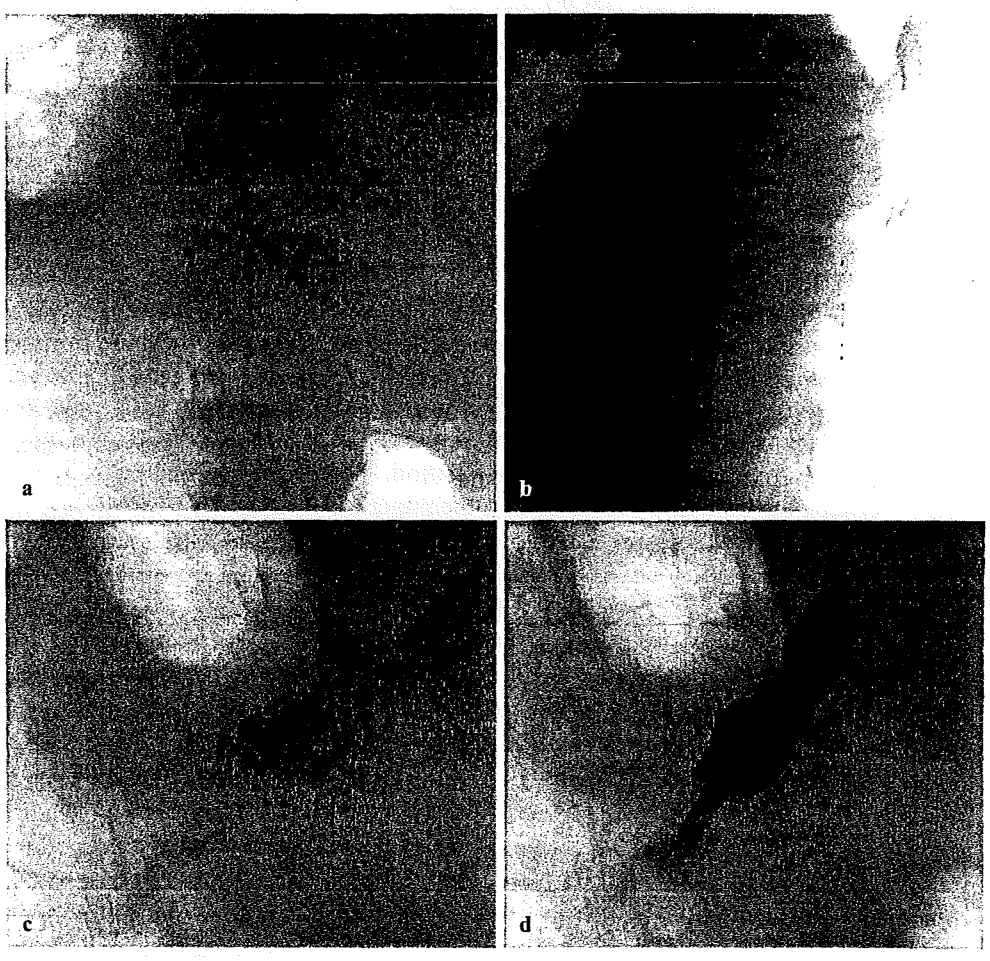

Fig. 2. Positioning. **a** In the frontal view, the ICM is aligned with the median of the vertebral body. **b** In the lateral view, the ICM is aligned with the anterior one-third median site of the vertebral body. **c** The C-arm is moved in a three-dimensional manner so the ICM is aligned with the center of the shadow of the vertebral arch pedicle. **d** The shadow of the puncture needle becomes a *dotted line* and is aligned with the ICM

body is aligned with the ICM (Fig. 2b). After carrying out these steps, the positioning of the isocenter marker in regard to the patient's position is completed. Consequently, regardless of how the C-arm rotates, the puncture target point is now aligned with the ICM at all times.

Next, the direction of the puncture direction is determined by rotating the C-arm in a three-dimensional manner so the ICM overlaps the center of the pediculus arcus vertebral image (Fig. 2c). With this step, the puncture direction is determined under fluoroscopy.

After confirming the cutaneous puncture site on the skin and administering local anesthesia, the puncture is performed while maintaining the puncture direction so the puncture needle overlaps the ICM in a point-like manner under fluoroscopy (Fig. 2d). When the needle reaches a depth of 1–2 cm in the vertebral arch pedicle, and the assistance of the needle is thus no longer required, the monitor is switched to the lateral fluoroscopic image, and the puncture needle is moved forward until the needle tip reaches the ICM (Fig. 3a). When moving the needle forward, a hammer is used as required. After the puncture needle tip has reached the ICM in the lateral image, the monitor is returned to the frontal fluoroscopic image to confirm that the puncture needle tip is aligned with the ICM (Fig. 3b), thereby completing the puncture by the ISOP method.

Materials

A total of 122 patients (224 vertebral bodies) underwent fluoroscopic PVP. They were then divided into three groups. Table 1 represents the characteristics of those groups. The first (group A) comprised 41 patients (73 vertebral bodies) who had undergone PVP by the ISOP method from January 2006 to March 2007. The second group (group B) comprised 58 patients (118 vertebral bodies) who had undergone PVP by the puncture simulation method from September 2004 to January 2006. The third group (group C) comprised 23 patients (33 vertebral bodies) who had undergone PVP without using the ICM from June 2002 to May 2004.

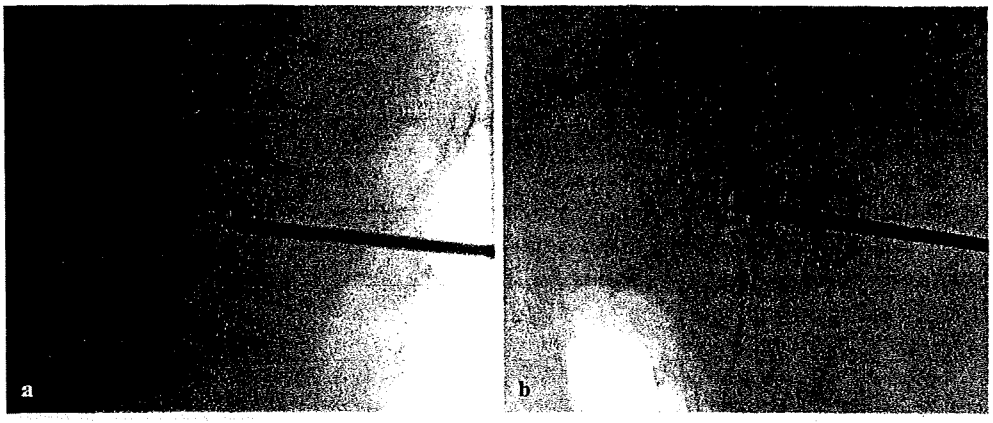

Fig. 3. Verification.
a Lateral view: the puncture needle tip overlaps the ICM.
b Frontal view: the puncture needle tip overlaps the ICM

Table 1. Summary of patients

Characteristic	ISOP method (group A)	Puncture simulation (group B)	Conventional method (group C)
Cases (vertebrae)	41 (73)	58 (118)	23 (33)
Male/female	8/33	11/47	9/14
Age (years), average/range	68.3/37–90	67.2/33–91	73.9/30–87
Location (case)	Th7 (1), Th8 (2), Th10 (3), Th11 (2), Th12 (12), L1 (18), L2 (14), L3 (10), L4 (9), L5 (2)	Th5 (1), Th6 (3), Th7 (2), Th8 (6), Th9 (8), Th10 (4), Th11 (10), Th12 (14), L1 (12), L2 (16), L3 (18), L4 (18), L5 (6)	Th8 (2), Th11 (1), Th12 (4), L1 (4), L2 (6), L3 (4), L4 (5), L5 (7)
Underlying disease (cases/vertebrae)			
Osteoporosis	34/58	45/81	11/15
Bone metastasis	7/15	13/37	11/17
Multiple myeloma			1/1

Methods

For all groups, we measured the success rate of the median puncture of the vertebral body (SR)[1,2] and the time required to perform a needle puncture successfully. The SR was evaluated by three radiologists during the procedure. It was judged by macroscopic evaluation of whether the needle tip reached the median of the vertebral body and by objective evaluation of whether the bone cement was distributed beyond the median of the vertebral body. These evaluations were done by using examples from previous observations of Kim et al.[1] For cases of failure, puncture was performed from the opposite side or from the same side after removing the needle. Fisher's exact test was used to evaluate all groups.

The procedure time for needle puncture was defined from the start of the positioning to puncture completion. The procedure time for needle puncture did not include the time needed to prepare the bone cement or the time needed to inject the cement. For a comparison of the puncture time, Mann-Whitney's U-test was used.

In group A, the puncture error, fluoroscopy time, and adverse events were further examined. Because the puncture target point with the ISOP method is determined by the operator's visual estimation during the procedure, it is not necessarily the anterior one-third median site of the vertebral body. When the patient is moved after the puncture direction is determined, a slight misalignment is likely to occur between the puncture target point and the ICM. Therefore, to evaluate the puncture error in the ISOP method, we verified where the puncture needle tip is located on the image obtained before the cement injection and measured the positional error between the puncture needle tip and the ideal puncture target point. For the error between the puncture needle tip and the ideal puncture target point, we measured the lateral direction of the axis in the frontal view and the craniocaudal direction of the axis in the lateral view.

For the fluoroscopy time during the procedure, the time between the positioning and rotation digital angiography immediately after the procedure was thus measured. The examination of adverse events was based on their presence or absence during the procedure.

A single plane C-arm of Infinix celeve VC (Toshiba Medical) was used for X-ray fluoroscopy. The puncture needle, an osteo-site bone biopsy needle (13 gauge, 15 cm; Cook, Spencer, IN, USA) was used. For injecting the cement preparation, Osteoject (Integra Neuro-Science, Plainsboro, NJ, USA) was used. PMMA (polymethylmethacrylate) was the bone cement, which was prepared by mixing 20 g of PMMA with 6 g of sterilized barium sulfate.

Table 2. Success rate ratio

Group	SR	Non-SR	Total
A	72	1	73
B	110	8	118
C	19	14	33
Total	201	23	224

SR, success rate

Results

Success rate of the median puncture of the vertebral body

The success rate (SR) for median puncture of the vertebral body was 98.6% (72/73) in group A, 93.2% (110/118) in group B, and 58% (19/33) in group C (Table 2). No significant differences were observed between groups A and B ($P = 0.15$). When comparing groups A and C, the SR was significantly higher in group A ($P < 0.05$).

In cases where a median puncture could not be successfully performed, either additional punctures were attempted from the opposite side or the same puncture was repeated. In all cases, satisfactory cement distribution to the lateral regions crossing the median was ultimately obtained.

Procedure time

The average procedure time for needle puncture for one vertebral body was 9.3 ± 3.8 min in group A, 11.2 ± 4.6 min in group B, and 30.9 ± 11.2 min in group C. No significant differences between groups A and B were observed regarding the puncture time ($P = 0.22$); however, the time was significantly shorter between groups A and C ($P < 0.01$).

Positional relation between the ideal puncture target point and the puncture needle tip—ISOP method

The average error in the horizontal direction was 1.52 ± 1.31 mm (maximum 5.92 mm), the average error in the ventrodorsal direction was 2.08 ± 1.50 mm (maximum 6.41 mm), and the average error in the craniocaudal direction was 1.87 ± 1.43 mm (maximum 5.81 mm). Figure 4 shows the positional relation between the ideal puncture target point and the puncture needle tip to each axis. As shown in Fig. 4b, we detected a tendency for the puncture needle tip to go slightly deeper toward the abdominal side of the vertebral body.

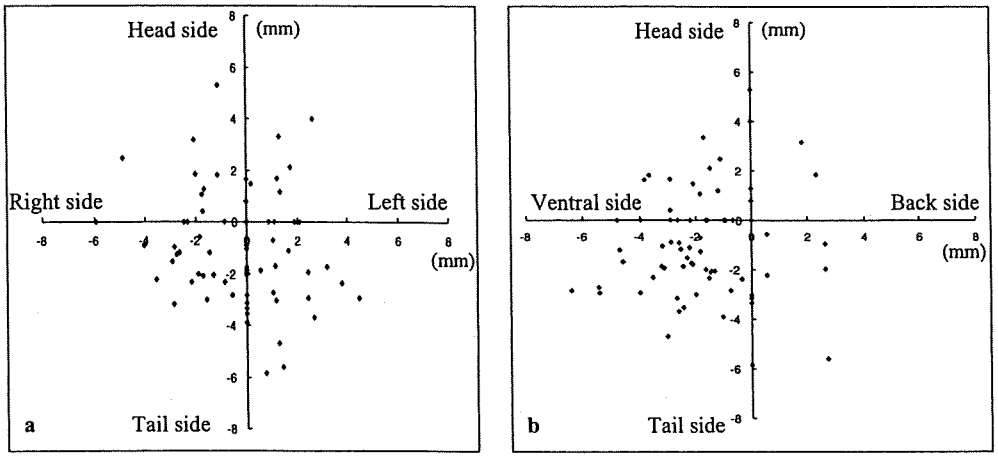

Fig. 4. Positional relation between the puncture needle tip and the puncture target point. **a** frontal view. **b** lateral view

Fluoroscopy time during the procedure—ISOP method

In group A, the average fluoroscopy times during the procedure were 5.8 ± 0.9 min for 23 cases of operating on one vertebral body, 8.97 ± 3.79 min for 8 cases of operating on two vertebral bodies, 9.33 ± 3.79 min for 4 cases of operating on three vertebral bodies, and 11.8 ± 2.83 min for 6 cases of operating on four vertebral bodies.

Adverse events—ISOP method

Two patients in group A had a fever after the procedure. Although the hospitalization period of these patients was extended by approximately 1 week, the symptoms were alleviated by antibiotic administration. No technique-related complications were observed.

Discussion

There have been only a few reported evaluations of PVP procedures, and most of them reported on cement distribution and leakage.[1–8] Many institutions select PVP using the bilateral transpedicular approach, thus expecting an even cement distribution within the vertebral body. Kim et al.[1] noted that if the unilateral transpedicular approach can achieve cement distribution across the median there are no differences in treatment effects compared to the bilateral transpedicular approach. In our examination, it was confirmed that by using the ISOP method the PVP success rate was 98.6%, and that even with the unilateral vertebral transpedicular approach bilateral cement distribution can be achieved if puncture is successfully performed with a target point of the anterior one-third median site of the vertebral body.

In group A, puncture had to be repeated in one case. In this case, it was attributed to body movement after positioning, whereby the ICM was misaligned from the puncture target point during the puncture. In this case, the ISOP method was applied again after removing the puncture needle. Favorable treatment effects were then obtained.

The puncture times were significantly shorter in group A than in group C, suggesting that the ISOP method contributes to a reduction of the puncture time in comparison to the conventional method.

In our hospital, before introducing the ISOP method, PVP had been implemented using the puncture simulation method.[2] With both the ISOP method and the puncture simulation method, there were no significant differences in the SR or the puncture time. Based on the above results, we speculate that no substantial differences exist between the ISOP method and the puncture simulation method. However, the puncture simulation method requires a preoperative CT examination and measurement of the puncture angle. Considering the labor hours and complexity, it is obvious that the ISOP method is a simpler, more useful puncture method.

Puncture accuracy in the ISOP method was an average of 2 mm in each of the horizontal, ventrodorsal, and craniocaudal directions. With this examination, except for case in which a second puncture was required owing to the patient's body movement (group A), the puncture needle tip reached the ICM in all cases, which is thus regarded as high puncture accuracy.

Reports on the amount of exposure and fluoroscopy time in the PVP are scarce.[10–12] Komemushi et al. have performed PVP by using the IVR-CT system and reported that the fluoroscopy time was 6.66 ± 2.45 min.[11] We used only a fluoroscopy device. The average fluoroscopy time for one vertebral body was 5.8 ± 0.9 min,

which was short, on average. In addition, Mehdizade et al. reported that the PVP fluoroscopy time under fluoroscopy was 10–60 min.[10] Compared to these reports, PVP under fluoroscopy by means of the ISOP method is believed to contribute to a significant reduction in the fluoroscopy time.

Conclusion

Compared to the conventional method, the ISOP method is thought to be a useful approach as it improves the PVP completion rate by using the unilateral vertebral arch pedicle approach; it also reduces the puncture time and fluoroscopy time. Thus, we speculate that the ISOP method is a more convenient technique than the puncture simulation method.

References

1. Kim AK, Jensen ME, Dion JE, Schweickert PA, Kaufmann TJ, Kallmes DF. Unilateral transpedicular percutaneous vertebroplasty: initial experience. Radiology 2002;222:737–41.
2. Kobayashi K, Takizawa K, Koyama M, Yoshimatsu M, Sakaino S, Nakajima Y. Unilateral transpedicular percutaneous vertebroplasty using puncture simulation. Radiat Med 2006;24:187–94.
3. Takizawa K, Yoshimatsu M, Nakajima Y, Sakaino S, Yagihashi K, Ogawa Y, et al. Development of a new support method for transpedicular punctures of the vertebral body: the isocenter puncture method. Cardiovasc Intervent Radiol 2007;30:757–60.
4. Koyama M, Takizawa K, Kobayashi K, Sasaka K, Hoshikawa Y, Nakaji S, et al. Initial experience of percutaneous vertebroplasty using single plane C-arm fluoroscopy for guidance. Radiat Med 2005;23:256–60.
5. Jensen ME, Evans AJ, Mathis JM, Kallmes, DF, Cloft HJ, Dion JE. Percutaneous polymethylmethacrylate vertebroplasty in the treatment of osteoporotic vertebral body compression fractures: technical aspects. AJNR Am J Neuroradiol 1997;18:1897–904.
6. Cotton A, Boutry N, Cortet B, Assaker R, Demondion X, Leblond D, et al. Percutaneous vertebroplasty: state of the art. Radiographics 1998;18:311–20.
7. Tohmeh AG, Mathis JM, Fenton DC, Levine AM, Belkoff SM. Biomechanical efficacy of unipedicular versus bipedicular vertebroplasty for the management of osteoporotic compression fractures. Spine 1999;24:1772–6.
8. Deramond H, Depriester C, Galibert P, LeGars D. Percutaneous vertebroplasty with polymethylmethacrylate: technique, indications, and results. Radiol Clin North Am 1998;36: 533–46.
9. Do HM, Kim BS, Marcellus ML, Curtis L, Marks MP. Prospective analysis of clinical outcomes after percutaneous vertebroplasty for painful osteoporotic vertebral body fractures. AJNR Am J Neuroradiol 2005;26:1623–8.
10. Mehdizade A, Lovblad KO, Wilhelm KE, Somon T, Wetzel SG, et al. Radiation dose in vertebroplasty. Neuroradiology 2004;46:243–5.
11. Komemushi A, Tanigawa N, Kariya S, Kojima H, Shomura Y, Sawada S. Radiation exposure to operators during vertebroplasty. J Vasc Interv Radiol 2005;16:1327–32.
12. Kallmes DF, O E, Roy SS, Piccolo RG, Marx WF, Lee JK, et al. Radiation dose to the operator during vertebroplasty: prospective comparison of the use of 1-cc syringes versus an injection device. AJNR Am J Neuroradiol 2003;24:1257–60.

ORIGINAL ARTICLE

ACTA RADIOLOGICA

Improvement in Respiratory Function by Percutaneous Vertebroplasty

N. TANIGAWA, S. KARIYA, H. KOJIMA, A. KOMEMUSHI, Y. SHOMURA, T. TOKUDA, Y. UENO, S. KUWATA, A. FUJITA, J. TERADA & S. SAWADA

Department of Radiology, Kansai Medical University Hirakata Hospital, Osaka, Japan; Department of Radiology, Kansai Medical University Takii Hospital, Osaka, Japan

Tanigawa N, Kariya S, Kojima H, Komemushi A, Shomura Y, Tokuda T, Ueno Y, Kuwata S, Fujita A, Terada J, Sawada S. Improvement in respiratory function by percutaneous vertebroplasty. Acta Radiol 2008;49:638–643.

Background: Percutaneous vertebroplasty (PVP) improves back pain and corrects spinal misalignment to some extent, and thus may improve respiratory function.
Purpose: To retrospectively investigate changes in respiratory function after PVP.
Material and Methods: 41 patients (mean age 72.0 years, range 59–86 years; 39 women, two men) who had undergone PVP for vertebral compression fractures (37 thoracic vertebral bodies [Th6–Th12] and 50 lumbar vertebral bodies [L1–L5]) caused by osteoporosis visited our hospital for follow-up consultation between January and June 2005. At this follow-up consultation, respiratory function testing, including percent forced vital capacity (FVC%) and percent forced expiratory volume in 1 s (FEV_1%), was performed. We retrospectively compared these values with those taken before PVP using a Wilcoxon signed-rank test.
Results: FVC% was 85.2±30.3% before PVP and 91.5±16.8% at follow-up (mean 10 months after PVP), which represented a significant difference ($P<0.003$). No significant difference in FEV_1% was detected. Regarding the number of treatment levels, that is, single vertebroplasty versus multiple vertebroplasty, no significant difference in improvement of FVC% was confirmed ($P=0.1$). FVC% was abnormally low (≤79%) before PVP in 16 patients and improved to within normal range postoperatively in six of these patients (38%).
Conclusion: PVP improves preoperatively decreased lung function, but this improvement takes time.

Key words: Osteoporosis; percutaneous vertebroplasty; respiratory function

Noboru Tanigawa, Department of Radiology, Kansai Medical University Hirakata Hospital, 2-3-1 Shinmachi, Hirakata, Osaka, 573-1191, Japan (fax. +81 72 804 2865, e-mail. tanigano@hirakata.kmu.ac.jp)

Accepted for publication February 24, 2008

Vertebral compression fracture due to osteoporosis causes not only back pain, but also spinal misalignment, particularly kyphosis. Kyphosis of the thoracic spine in turn causes rib cage deformity. In this manner, vertebral compression fracture reduces the activities of daily living (ADL) (1), causes respiratory dysfunction due to rib cage deformity, and increases the prevalence of lung diseases (2, 3).

Mortality rates in osteoporotic women who have been clinically diagnosed with vertebral compression fracture are 15% higher than in those without compression fracture (4). Furthermore, mortality rates are 23–34% higher in osteoporotic women with severe multiple compression fractures or kyphosis than in women without these conditions, and this is primarily related to compromised pulmonary function as a result of thoracic and lumbar vertebral fractures (2).

Percutaneous vertebroplasty (PVP) was first reported in 1987 (5). Since then, PVP has been performed to alleviate pain caused by various types of vertebral compression fracture, and dramatic effectiveness in this regard has led to frequent use (6–9). PVP is also useful for back pain caused by compression fractures due to osteoporosis and has contributed greatly to improvements in ADL (6, 10, 11).

Since PVP improves back pain and corrects spinal misalignment to some extent, we hypothesized that respiratory function might also be

informa
healthcare

DOI 10.1080/02841850802010758

improved, reducing the incidence of respiratory complications and increasing life expectancy. The present study thus investigated the long-term benefits of PVP with regard to respiratory function.

Material and Methods

Patients

The indication for PVP was back pain caused by vertebral body compression fracture, with pain on percussion of the vertebral spinous process. In cases with multiple compression fractures in which percussion pain of the spinous process was unclear, physical examination was performed using fluoroscopy. Patients with back pain attributed to myelopathy or radiculopathy resulting from stenosis of the vertebral canal or narrowing of the intervertebral foramen were excluded.

This study comprised 41 patients (mean age 72.0 years, range 59–86 years; 39 women, two men) who had vertebral compression fractures caused by osteoporosis and had undergone PVP to treat 37 thoracic vertebral bodies (Th6–Th12) and 50 lumbar vertebral bodies (L1–L5) before respiratory function testing. PVP had been performed to treat one vertebral body in 13 patients, two vertebral bodies in 14 patients, three vertebral bodies in 10 patients, and four vertebral bodies in four patients (Table 1).

These 41 patients had undergone PVP at our institution and visited our hospital for follow-up consultation between January and June 2005; one patient who had undergone PVP at our hospital in the past and visited the outpatient clinic due to a new compression fracture during the study period was excluded. At this follow-up consultation, respiratory function testing was performed in all 41 patients. Mean duration between PVP and respiratory function testing was 10 months (range 1–24 months). Preprocedural pulmonary function was retrospectively reviewed. Our institution does not require institutional review board approval for retrospective reviews.

At our institution, respiratory function testing was performed 1–3 days before PVP in all patients. Values from respiratory function testing were not included in the exclusion criteria. Furthermore, patients who underwent PVP during this study period (January to June 2005) underwent additional respiratory function testing the day after PVP.

PVP procedure

All procedures were performed by either one of the authors (N.T.), who had 7 years' experience in PVP, or by a fellowship trainee under the supervision of N.T. PVP was performed under combined computed tomography (CT) and fluoroscopic guidance (Advantex LCA+ACT; GE Medical Systems, Milwaukee, Wisc., USA). Thirty minutes preoperatively, 10 mg of morphine hydrochloride (Sankyo, Tokyo, Japan), 0.5 mg of atropine sulfate (Tanabe, Osaka, Japan), and 25 mg of hydroxyzine hydrochloride (Pfizer Japan, Tokyo, Japan) was administered intramuscularly. Local anesthesia with 10 ml of 1% lidocaine (AstraZeneca, Osaka, Japan) was performed from the skin to the periosteum of the pedicle using a 22G Cathelin needle (Terumo Europe, Leuven, Belgium) under fluoroscopic guidance. After orientation of the puncture needle was confirmed on CT and aligned with the Cathelin needle, a 13G bone biopsy needle (Osteo-Site Bone Biopsy Needle Murphy M2; Cook, Bloomington, Ind., USA) was advanced into the pedicle of the vertebral arch. A unilateral transpedicular approach was selected for all cases. CT was repeated, and after confirming orientation of the biopsy needle, the visualization modality was changed to lateral fluoroscopy and the bone biopsy needle was advanced to the anterior third of the vertebral body close to the midline.

Intraosseous venography was performed using 1–5 ml of iopamidol (Iopamiron 300; Schering Japan, Osaka, Japan) or 5–20 ml of carbon dioxide to confirm that the needle was not positioned within a direct venous anastomosis to the central or epidural veins. Subsequently, 20 g of methyl methacrylate powder (Osteobond copolymer bone cement; Zimmer, Warsaw, Ind., USA) was mixed with 5 g of barium sulfate powder (Horii Pharmaceutical, Osaka, Japan) that had been sterilized with dry heat to increase opacity. Next, 10 ml of liquid methyl methacrylate monomer was added to the powder, and the mixture was blended to a toothpaste-like consistency, producing polymethyl methacrylate (PMMA). Using 1-ml syringes, PMMA was injected under lateral fluoroscopic guidance. PMMA injection was terminated when adequate filling of the vertebral body was achieved or if leakage occurred. If leakage occurred, the needle was repositioned and additional PMMA was injected to fill the remaining part of the vertebral body. The needle was then removed, and all patients were observed in a supine position for 2 hours.

Pulmonary function testing

Respiratory function was assessed using percent forced vital capacity (FVC%), representing restrictive ventilatory disturbance, and percent forced

Table 1. Measurements of pulmonary function.

Patients No./sex/age (years)	Level	FVC%			FEV_1%		
		Pre-PVP (%)	1 day after (%)	At follow-up (%)	Pre-PVP (%)	1 day after (%)	At follow-up (%)
1/F/71	L1, L2, L3	94.8		90.7	80.7		78.6
2/F/71	T12, L4, L5	126.2		123	79.3		75.9
3/F/64	L1, L2	83.1		79.7	60.7		58.2
4/F/75	L1, L2, L3	109.1		93	85.9		88.5
5/F/75	T12	100		93.2	77.8		76.6
6/F/76	T7	61.9		88.3	66.9		69.4
7/F/75	T8, T9	94.9		93	93.1		88.5
8/F/73	T10, T11	79.9		95.6	74.7		75.5
9/F/65	L1	90.7		99.3	88		85.4
10/F/77	T12	60.2		66.6	84.7		73.7
11/F/85	L2	77.8		107.6	78.4		79.7
12/F/73	T9, T10	87.4		95.6	80.4		75.5
13/F/62	T12, L1, L2	91.9		105.5	86.4		87
14/F/71	L1	75.8	88.4	88.4	43.6	47.3	47.3
15/F/71	L1, L2, L3	104.7	97.9	104.1	80.6	82.5	81.7
16/F/73	T9, T10, T11	119.8	100.1	105.9	73.6	74.6	79.9
17/F/68	T9, T10, T11, T12	98.4	107.6	112.3	92.9	88.3	85.3
18/F/78	T6, T7, T8, T9	63.8	75.9	78.2	73.7	66	62.4
19/F/86	T11, T12	50.4	80.3	56.3	70.9	72	73.9
20/F/66	L2	61.3	63.1	80.5	76.7	77.2	77.8
21/F/71	T12, L1, L3	104.7		106.4	80.3		92.3
22/F/66	T12, L1, L2, L3	112.4		122.4	81.9		79.9
23/F/59	T12, L1	66.7		72.6	77.2		87.9
24/F/72	L3	79.5		103.3	83.8		79.7
25/F/72	L1, L3, L4, L5	58.3		83	78.6		75.1
26/F/70	L4, L5	109.7		124.1	83.1		77.8
27/F/74	T11, T12, L1	91.2		94.2	79.8		84.6
28/F/73	L1	84.9		72.5	85.5		98.6
29/M/76	L2, L3	55.2		59.7	83.7		85.5
30/F/78	L1, L4, L5	99.8		92.1	66.7		71.3
31/M/77	T12	77.5		93.8	82.5		74.6
32/F/76	L1, L3	81.4		93.1	73.5		93.1
33/M/61	L4	98.2		99.8	82.2		82.3
34/F/74	L4, L5	47.2		74	72.1		71.9
35/F/86	T11, T12	50.4	80.3	56.3	70.9	72	73.9
36/F/68	T11, T12	84.7	84.9	94.1	85.6	84.4	74.2
37/F/84	T12, L1	108.6	106.3	100.4	73.1	72.1	76.8
38/F/65	T11	75.8		84.9	48.2		46.8
39/F/72	T11, T12, L1	94.5	69.7	88.7	67.6	62.1	76.2
40/F/64	L1	69.6		71.9	81.5		78.8
41/F/64	L3, L4	110.5	105.9	107.9	72.2	76.3	81.1

FVC%: percent forced vital capacity; FEV_1%: percent forced expiratory volume in 1 s.

expiratory volume in 1 s (FEV_1%), representing obstructive ventilatory disturbance.

FVC and FEV_1 were measured using a spirometer (System 9; Minato Ika, Osaka, Japan) with an online computer. Spirometry was performed at least three times for FEV_1 and FVC, which fulfilled the criteria of the American Thoracic Society (12).

Statistical analysis

In all patients, severity of back pain was assessed using a visual analog scale (VAS) of 0–10, with 0 representing no pain and 10 representing the worst pain imaginable, before PVP and at the time of respiratory function testing.

Subjects were divided into single-vertebroplasty and multiple-vertebroplasty groups. The single-vertebroplasty group consisted of patients in whom one vertebra was treated, while the multiple-vertebroplasty group comprised patients who received treatment for two or more vertebrae. FVC% before and after PVP was compared between these two groups using the Wilcoxon signed-rank test. The Mann-Whitney U test was used to compare the degree of improvement in FVC%.

In addition, to ascertain differences in the efficacy of PVP, the degree of improvement in VAS ([VAS score before PVP] – [VAS score at respiratory function testing]) was compared between groups using the Mann-Whitney U test.

Furthermore, FVC% was divided into the following four grades: <60%, 60–79%, 80–99%, and 100%. Frequency distribution of FVC% was compared before and after PVP.

Subjects were also divided into three groups with respect to treatment level: thoracic group, thoracolumbar group, and lumbar group. Cement injection was performed only on thoracic vertebrae in the thoracic group, on both thoracic and lumbar vertebrae in the thoracolumbar group, and on lumbar vertebrae in the lumbar group. Among these groups, FVC% was compared before PVP and at one time during the follow-up period using the Wilcoxon signed-rank test. In addition, to ascertain differences in the efficacy of PVP among groups, the degree of improvement in VAS ([VAS score before PVP] – [VAS score at respiratory function testing]) was compared among groups using the Mann-Whitney U test.

Results

PVP was successfully performed in all cases. No complications were encountered, and no new shadows in the lung parenchyma, such as cement emboli, were identified on postprocedural chest radiography.

Mean VAS was 7.0 ± 2.3 ($n=41$) before PVP, 1.9 ± 2.4 ($n=12$) the day after PVP, and 1.5 ± 1.4 ($n=41$) at the time of follow-up.

FVC% and FEV_1% before, 1 day after, and at a mean of 10 months after PVP are displayed in Table 2. A significant difference in FVC% was evident between before PVP and a mean of 10 months after PVP ($P<0.003$). However, no significant difference was seen in FEV_1%.

Table 2. Changes in FVC% and FEV_1% for all study patients.

Parameters	FVC%	FEV_1%
Before PVP ($n=41$)	85.2 ± 30.3*	77.0 ± 9.98
1 day after PVP ($n=12$)	88.4 ± 15.1	72.9 ± 10.9
At follow-up ($n=41$)	91.5 ± 16.8*	77.6 ± 10.4

Data are expressed as mean ± standard deviation.
FVC%: percent forced vital capacity; FEV_1%: percent expiratory volume in 1 s; PVP: percutaneous vertebroplasty.
*Statistically significant difference ($P<0.01$).

Single vertebroplasty vs. multiple vertebroplasty

Thirteen patients had single vertebroplasty and 28 multiple. Table 3 shows FVC% before PVP and at follow-up for the single- and multiple-vertebroplasty groups. In both groups, significant differences in FVC% were identified (single-vertebroplasty group, $P=0.02$; multiple-vertebroplasty group, $P=0.05$). However, degree of improvement in FVC% following PVP was 10.5 ± 12.6% for the single group and 4.4 ± 10.6% for the multiple group, with no significant difference observed between the groups ($P=0.1$). Moreover, the degree of improvement in pain following PVP was 5.2 ± 3.1 for the single group and 6.0 ± 2.8 for the multiple group. No significant difference was observed between the groups ($P=0.4$).

Treatment at spinal level

Regarding spinal level, the thoracic group included 19, the thoracolumbar group eight, and the lumbar group 14 patients. Mean FVC% before PVP and 10 months after PVP for the thoracic, thoracolumbar, and lumbar groups are shown in Table 4. Only the thoracic group displayed a significant difference ($P=0.02$).

Degree of improvement in pain following PVP was 4.6 ± 3.1 for the thoracic group, 6.1 ± 2.9 for the thoracolumbar group, and 5.8 ± 2.9 for lumbar group, with no significant difference apparent among these groups.

Changes in frequency distribution of FVC%

Table 5 shows the frequency distribution of FVC% before PVP and FVC% at follow-up (mean follow-up, 10 months). FVC% was abnormally low (=79%) before PVP in 16 patients and normalized postoperatively in six of these patients (38%).

Table 3. Relationship between changes in FVC% and the number of treated vertebral bodies.

	Before PVP	At follow-up	*P* value
Single-vertebroplasty group	77.9 ± 13.0	88.5 ± 12.8	0.02
Multiple-vertebroplasty group	88.6 ± 22.4	92.2 ± 18.4	0.05

Data are expressed as mean FVC% ± standard deviation (%).
FVC%: percent forced vital capacity; FEV_1%: percent expiratory volume in 1 s; PVP: percutaneous vertebroplasty.
P value was obtained by Wilcoxon signed-rank test between before and during follow-up.

Table 4. Relationship between changes in FVC% and treatment level.

	Before PVP	At follow-up	*P* value
Thoracic vertebrae group	83.8±19.3	90.8±15.7	0.02
Thoracic and lumbar vertebrae group	99.5±17.8	101.1±16.9	0.48
Lumber vertebrae group	78.9±20.3	86.7±17.9	0.06

Data are expressed as mean FVC%±standard deviation (%).
FVC%: percent forced vital capacity; FEV_1%: percent expiratory volume in 1 s; PVP: percutaneous vertebroplasty.
P value was obtained by Wilcoxon signed-rank test between before and during follow-up.

Changes in FVC% for patients with decreased lung function (FVC% <79)

FVC% for these 16 patients is shown in Table 6. A significant difference in FVC% was observed between before PVP and 1 day after PVP ($P=0.043$), and between before PVP and 10 months after PVP ($P<0.001$).

Discussion

In our study, 16 of the 41 patients displayed low FVC%, or decreased lung function, before PVP. In these 16 patients, improvement in ventilatory disturbance was achieved immediately after PVP and was maintained thereafter. Furthermore, in six of the 16 patients (38%), FVC% normalized after PVP. In patients with compression fractures due to osteoporosis, PVP effectively improves back pain (6–9). Costal movements that are restricted before PVP due to back pain subsequently improve after PVP due to alleviation of pain. Furthermore, PVP improves reduced vertebral body height due to compression fracture (13, 14), thereby alleviating local kyphosis (15).

For the entire subject group, FVC% was improved only slightly immediately after PVP, but improved to a greater degree at a mean follow-up of 10 months. This suggests that decreased lung function improves even in patients who do not display defined decreased lung function preoperatively, but this improvement takes time. In other words, PVP eliminates back pain immediately after the procedure. Among patients who displayed decreased lung function preoperatively, reduced pain and greater costal movements directly improved FVC%, and among those who did not exhibit decreased lung function preoperatively, PVP improved back pain and increased daily exercise tolerance, allowing indirect improvements to ventilatory capacity. That is, increased daily exercise works as rehabilitation for thoracic cage movement.

Table 5. Frequency distribution of FVC%.

FVC%	0–59%	60–79%	80–99%	100% or more
Before PVP ($n=41$)	5 (12)	11 (27)	15 (37)	10 (24)
At follow-up ($n=41$)	2 (5)	8 (20)	19 (46)	12 (29)

Data are number of patients. Numbers in parentheses are percentages.
FVC%: percent forced vital capacity; PVP: percutaneous vertebroplasty.

Table 6. Changes in FVC% for patients with decreased lung function.

Parameters	FVC%
Before PVP ($n=16$)	65.7±11.3*#
1 day after PVP ($n=16$)	77.6±9.3*
At follow-up ($n=16$)	80.9±15.5#

Data are expressed as mean value±standard deviation.
FVC%: percent forced vital capacity; PVP: percutaneous vertebroplasty.
*Statistically significant difference ($P=0.04$).
#Statistically significant difference ($P<0.01$).

No significant differences in degree of pain improvement were seen between the single- and multiple-vertebroplasty groups, and FVC% significantly improved for both groups. These results might be explained by the fact that improvements in decreased lung function primarily resulted from improvements in pain.

The three spinal-level groups displayed no significant differences in degree of pain improvement, and FVC% significantly improved only for the thoracic group. This might be explained by the fact that, as described above, decreased lung function improves when rib cage volume, costal movement, and pain improve, and the impact of these changes was greater for the thoracic group.

Pain improved in all of our patients, so statistical confirmation could not be achieved of whether pain alleviation contributed to improvements in decreased lung function. However, pain, particularly back pain, can easily be considered to restrict costal movement. We are therefore certain that pain alleviation represents one of the factors leading to improvements in decreased lung function.

We used forced vital capacity instead of vital capacity to evaluate restrictive ventilatory disturbance. We consider that back pain due to compression is one of the major factors contributing to the induction of obstructive ventilatory disturbance. However, full inspiration followed by forced

expiration is needed to measure FVC. Patients with back pain can perform slow inspiration and expiration, but rapid inspiration and expiration are not possible. We therefore consider that FVC is more sensitive than vital capacity when comparing restrictive lung function between pre- and post-PVP.

The present study displayed several limitations. The first is the lack of a control group. Patients who develop acute compression fractures are more likely to display decreased lung function, and as these fractures heal, pulmonary function would likely improve. Second, because of the retrospective nature of this study, the number of patients in whom respiratory function was assessed soon after PVP was low.

In conclusion, although the most important goal of PVP is to alleviate pain, the present study clarified that PVP also improves decreased lung function. Such improvements could lower the incidence of pulmonary complications, thus increasing the clinical significance of PVP.

References

1. Gold D. The clinical impact of vertebral fractures: quality of life in woman with osteoporosis. Bone 1996; 18 Suppl 3:185S–9S.
2. Leech JA, Dulberg C, Lellie S, Pattee L, Gay J. Relationship of lung function to severity of osteoporosis in women. Am Rev Respir Dis 1990;141:68–71.
3. Schlaich C, Minne HW, Bruckner T, Wagner G, Gebest HJ, Grunze M, et al. Reduced pulmonary function in patients with spinal osteoporotic fractures. Osteoporosis Int 1998;8:261–7.
4. Cooper C, Atkinson EJ, Jacobsen SJ, O'Fallon WM, Melton LJ. Population-based study of survival after osteoporotic fractures. Am J Epidemiol 1993;137: 1001–5.
5. Galibert P, Deramond H, Rosat P, Le Gars D. Preliminary note on the treatment of vertebral angioma by percutaneous acrylic vertebroplasty. [In French] Neurochirugie 1987;33:166–8.
6. Evans AJ, Jensen ME, Kip KE, DeNardo AJ, Lawler GJ, Negin GA, et al. Vertebral compression fractures: pain reduction and improvement in functional mobility after percutaneous polymethylmethacrylate vertebroplasty – retrospective report of 245 cases. Radiology 2003;226:366–72.
7. Hodler J, Peck D, Gilula LA. Midterm outcome after vertebroplasty: predictive value of technical and patients-related factors. Radiology 2003;227:662–8.
8. Mathis JM, Barr JD, Belkoff SM, Barr MS, Jensen ME, Deramond H. Percutaneous vertebroplasty: a developing standard of care for vertebral compression fractures. Am J Neuroradiol 2001;22:373–81.
9. Calmes V, Vallee JN, Rose M, Chiras J. Osteoblastic and mixed spinal metastases: evaluation of the analgesic efficacy of percutaneous vertebroplasty. Am J Neuroradiol 2007;28:570–4.
10. Kallmes DF, Jensen ME. Percutaneous vertebroplasty. Radiology 2003;229:27–36.
11. Serra L, Kermani FM, Panagiotopoulos K, De Rosa V, Vizioli L. Vertebroplasty in the treatment of osteoporotic vertebral fractures: results and functional outcome in a series of 175 consecutive patients. Minim Invasive Neurosurg 2007;50:12–7.
12. American Thoracic Society. Standardization of spirometry. Am Rev Respir Dis 1987;136:1285–98.
13. Hiwatashi A, Moritani T, Numaguchi Y, Westesson PL. Increase in vertebral body height after vertebroplasty. Am J Neuroradiol 2003;24:185–9.
14. Teng MM, Wei CJ, Wei LC, Luo CB, Lirng JF, Chang FC, et al. Kyphosis correction and height restoration effects of percutaneous vertebroplasty. Am J Neuroradiol 2003;24:1893–900.
15. Carlier RY, Gordji H, Mompoint DM, Vernhet N, Feydy A, Vallee C. Osteoporotic vertebral collapse: percutaneous vertebroplasty and local kyphosis correction. Radiology 2004;233:891–8.

Cardiovasc Intervent Radiol (2008) 31:1174–1177
DOI 10.1007/s00270-008-9325-5

CLINICAL INVESTIGATION

Intraosseous Venography with Carbon Dioxide in Percutaneous Vertebroplasty: Carbon Dioxide Retention in Renal Veins

Atsushi Komemushi · Noboru Tanigawa · Shuji Kariya · Hiroyuki Kojima · Yuzo Shomura · Takanori Tokuda · Motoo Nomura · Jiro Terada · Minoru Kamata · Satoshi Sawada

Received: 15 January 2008 / Accepted: 28 February 2008 / Published online: 21 March 2008

Abstract The objective of the present study was to determine the frequency of gas retention in the renal vein following carbon dioxide intraosseous venography in the prone position and, while citing references, to examine its onset mechanisms. All percutaneous vertebroplasties performed at our hospital from January to December 2005 were registered and retrospectively analyzed. Of 43 registered procedures treating 79 vertebrae, 28 procedures treating 54 vertebrae were analyzed. Vertebral intraosseous venography was performed using carbon dioxide as a contrast agent in all percutaneous vertebroplasty procedures. In preoperative and postoperative vertebral CT, gas retention in the renal vein and other areas was assessed. Preoperative CT did not show gas retention (0/28 procedures; 0%). Postoperative CT confirmed gas retention in the renal vein in 10 of the 28 procedures (35.7%). Gas retention was seen in the right renal vein in 8 procedures (28.6%), in the left renal vein in 5 procedures (17.9%), in the left and right renal veins in 3 procedures (10.7%), in vertebrae in 22 procedures (78.6%), in the soft tissue around vertebrae in 14 procedures (50.0%), in the spinal canal in 12 procedures (42.9%), and in the subcutaneous tissue in 5 procedures (17.9%). In conclusion, in our study, carbon dioxide gas injected into the vertebra frequently reached and remained in the renal vein.

Keywords Interventional radiology · Vertebroplasty · Carbon dioxide · Intraosseous venography · Spine

A. Komemushi (✉) · N. Tanigawa · S. Kariya · H. Kojima · Y. Shomura · T. Tokuda · M. Nomura · J. Terada · M. Kamata · S. Sawada
Department of Radiology, Kansai Medical University, 2-3-1 Shinmachi, Hirakata, Osaka 573-1191, Japan
e-mail: kome64@yo.rim.or.jp

Introduction

The use of intraosseous venography in percutaneous vertebroplasty remains controversial [1–6]. Intraosseous venography enables determination of whether a needle tip is inside the vertebra, whether a needle communicates with the intravertebral clefts, and macroscopic movements of bone fragments; demonstrates direct filling of veins leading to the epidural space without first passing through bone and intertrabecular spaces; and demonstrates the extravertebral pathway of contrast medium leakage. On the other hand, the disadvantages associated with intraosseous venography are that residual positive contrast medium in the vertebra hinders bone cement injection when there is a difference in viscosity between contrast medium and bone cement, and the flow of bone cement cannot be predicted [3–6]. When performing percutaneous vertebroplasty, we use carbon dioxide, a negative contrast medium, in intraosseous venography [1]. While the imaging ability of carbon dioxide is inferior to that of nonionic positive contrast media, because carbon dioxide is a negative contrast medium, it does not hinder bone cement injection if it remains in the vertebra.

Following carbon dioxide intraosseous venography in the prone position, when CT is performed postoperatively to determine the distribution of bone cement, we have sometimes seen gas retention in the renal vein. To the best of our knowledge, there have been no reports of gas retention in the renal vein following carbon dioxide venography. The objective of the present study is to determine the frequency of gas retention in the renal vein following carbon dioxide intraosseous venography in the prone position and, while citing references, to examine its onset mechanisms.

Materials and Methods

All percutaneous vertebroplasties performed at our hospital from January to December 2005 were registered and retrospectively analyzed. The total number of all percutaneous vertebroplasty procedures in this period was 43. Preoperative vertebral CT was performed to determine puncture route, postoperative vertebral CT was performed to confirm bone cement distribution, and procedures where the left and right renal hilar regions were depicted were chosen for further analysis. Of 43 registered procedures treating 79 vertebrae, 28 procedures treating 54 vertebrae (Th7, 1; Th11, 5; Th12, 10; L1, 13; L2, 12; L3, 11; L4, 2; and L5, 1) were analyzed. All procedures included at least one vertebra from Th12 to L3.

Percutaneous vertebroplasties were performed using an IVR-CT system (Advantx-ACT; GE Medical Systems, Milwaukee, WI, USA), which is a combination of angiographic equipment and CT equipment on a single fluoroscopy table. After intramuscular injection of 25 mg of hydroxyzine hydrochloride (Atarax P; Pfizer Japan Inc., Tokyo), 0.5 mg of atropine sulfate (Tanabe Seiyaku Co., Ltd., Osaka, Japan) and 10 mg of morphine hydrochloride (Sankyo Co., Ltd., Tokyo), the patient was positioned prone on the fluoroscopy table. Preoperative vertebral CT was performed in order to reference the puncture site and angle. The skin overlying the vertebral body to be injected was cleaned and draped. The skin, subcutaneous tissues, and periosteum over the pedicle to be punctured were then anesthetized with 1% lidocaine hydrochloride (Xylocaine polyamp, 1%; AstraZeneca KK, Osaka, Japan) using a 22 G × 70-mm Cathelin Needle (Terumo Europe N.V., Leuven, Belgium), with reference to CT images and lateral fluoroscopic guidance, and the needle tip was retained adjacent to the pedicle. CT was then performed to confirm the needle location. Using the needle as a guide, a 13-G needle (Osteo-site Bone Biopsy Needle Murphy M2; length, 10 cm; Cook Inc., Bloomington, IN, USA) was advanced without fluoroscopic guidance until its tip penetrated the cortex. CT was again performed to verify the needle position. Under lateral fluoroscopic guidance, the needle was then advanced into the vertebral body. Ideally, the tip of the needle was placed in the anterior third of the vertebral body, close to the midline. More posterior needle positions occasionally had to be accepted when treating severely compressed vertebral bodies with steep pedicle angulation.

Venography was then performed using carbon dioxide (CO_2) as a contrast agent. CO_2 was drawn from a CO_2 generator through a sterile filter into a 10- or 20-ml syringe (Gaster; Asahi Keiki Co., Osaka, Japan). After connecting the syringe containing CO_2 to the bone biopsy needle via 50 cm of extensible tubing, the operator manually injected CO_2 while keeping as far from the fluoroscopic field as possible. Frontal and lateral venograms were obtained using digital subtraction angiography (DSA). The amount of CO_2 used in venography was 10 ml for thoracic and 20 ml for lumbar vertebrae [1].

After this, 20 g of methylmethacrylate powder (Osteobond copolymer bone cement; Zimmer, Warsaw, IN, USA) was mixed with 5 g of dry heat-sterilized barium sulfate powder (Horii Pharmaceutical Ind., Ltd., Osaka, Japan) to increase its opacity [7]. Next, 10 ml of liquid methylmethacrylate monomer was added to the powder, and the resulting polymethylmethacrylate (PMM) mixture was blended to a toothpaste-like consistency. The PMM was loaded into a 10-ml syringe (Terumo Corp., Tokyo) and then backfilled into screw-type 1-ml syringes or the Bone Cement Injector system, ensuring that air was expelled from the PMM.

The PMM was injected under lateral fluoroscopic guidance. Injection was terminated when adequate filling of the vertebral body was achieved or when leakage outside the vertebral body occurred. When leakage occurred, the needle was repositioned and additional PMM was injected to fill the remaining part of the vertebral body. The needle was then removed, and postoperative vertebral CT was performed to confirm PMM distribution. After the CT procedure, all patients were observed in the supine position for 2 h.

In preoperative and postoperative vertebral CT, gas retention in the renal vein and other areas was assessed.

Results

Preoperative CT did not show gas retention (0/28 procedures: 0%).

Postoperative CT confirmed gas retention in the renal vein in 10 of the 28 procedures (35.7%). Gas retention was seen in the right renal vein in 8 of the 28 procedures (28.6%), in the left renal vein in 5 of the 28 procedures (17.9%), and in the left and right renal veins in 3 of the 28 procedures (10.7%) (Fig. 1).

With regard to gas retention in areas beside the renal vein, gas retention was seen in vertebrae in 22 of the 28 procedures (78.6%), in the soft tissue around vertebrae in 14 of the 28 procedures (50.0%), in the spinal canal in 12 of the 28 procedures (42.9%), and in the subcutaneous tissue in 5 of the 28 procedures (17.9%) (Table 1).

Discussion

When carbon dioxide, a negative contrast medium, is used for intraosseous venography during percutaneous

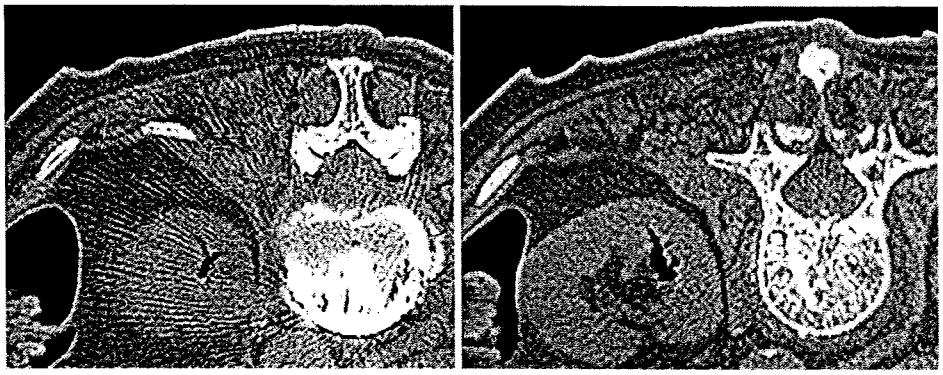

Fig. 1 CT images following carbon dioxide intraosseous venography in the prone position

Table 1 Locations where gas retention in the renal veins was seen (n = 28 procedures)

	Right renal hilus	Left renal hilus	Inside vertebra	Soft tissue around vertebra	Inside spinal tube	Subcutaneous tissue
Preoperative CT	0	0	0	0	0	0
Postoperative CT	8 (28.6%)	5 (17.9%)	22 (78.6%)	14 (50.0%)	12 (42.9%)	5 (17.9%)

vertebroplasty, even if the contrast medium remains inside the vertebra, bone cement injection is not hindered. We have observed gas retention in the renal hilus following carbon dioxide intraosseous venography. To the best of our knowledge, there have been no reports of gas retention in the renal hilus following carbon dioxide intraosseous venography. In the present study, we investigated the frequency of gas retention in the renal hilus following carbon dioxide intraosseous venography in the prone position; and CT after intraosseous venography showed gas retention in the renal vein in 10 of the 28 procedures (35.7%).

Carbon dioxide injected into the vertebra travels to extravertebral veins via the basivertebral veins. On the dorsal side of the vertebra, the basivertebral veins communicate with the anterior internal vertebral venous plexus on the anterior surface of the spinal canal, and on the ventral side of the vertebra, the basivertebral veins communicate with the anterior external vertebral venous plexus on the anterior surface of the vertebra. These venous plexuses communicate with the inferior vena cava via the intercostal and lumbar veins, and the anterior external vertebral venous plexus communicates directly with the inferior vena cava [8]. As the renal vein communicates with the lumbar veins and inferior vena cava, carbon dioxide gas injected in the vertebra reaches the renal vein via these pathways. These pathway veins are characterized by a lack of venous valves, thin walls, and easily altered flow [9].

Carbon dioxide tends to travel upward [10]. As the kidney is located on the dorsal side of the trunk in the superior direction, the prone position allows the carbon dioxide to travel to the renal vein. In addition, because the viscosity of carbon dioxide is low, it can easily flow backward through vessels [10].

When performing carbon dioxide intraosseous venography in the prone position, the frequency of gas retention in the renal vein was relatively high, at 35.7%; this is because there are communicating vessels from the spine to the renal vein, the prone position allows carbon dioxide to travel to the kidney, and the low viscosity of carbon dioxide increases the likelihood of backward flow through the veins.

Bone cement leakage is an important complication of percutaneous vertebroplasty. When injecting bone cement into the vertebra, cement leakage into a vein can cause an embolus. Chung et al. reported cement embolization of the renal vein as an extremely rare complication of percutaneous vertebroplasty, but its onset mechanism has not been clarified [11]. In our study, carbon dioxide gas injected into the vertebra frequently reached and remained in the renal vein. Because bone cement differs from carbon dioxide in terms of viscosity and specific gravity, renal vein embolization due to bone cement is thought to be rare. The present study may aid in the clarification of the onset mechanisms of renal vein embolization due to bone cement, which is a rare complication of percutaneous vertebroplasty.

References

1. Tanigawa N, Komemushi A, Kariya S et al (2005) Intraosseous venography with carbon dioxide contrast agent in percutaneous vertebroplasty. AJR 184:567–570
2. Jansen ME, Evans AJ, Mathis JM et al (1997) Percutaneous polymethylmethacrylate vertebroplasty in the treatment of osteoporotic vertebral body compression fractures: technical aspect. Am J Neuroradiol 18:1897–1904
3. McGraw JK, Heatwole EV, Strnad BT et al (2002) Predictive value of intraosseous venography before percutaneous vertebroplasty. J Vasc Interv Radiol 13:149–153

4. Gaughen JR Jr, Jensen ME, Schweickert PA et al (2002) Relevance of antecedent venography in percutaneous vertebroplasty for the treatment of osteoporotic compression fractures. Am J Neuroradiol 23:594–600
5. Vasconcelos C, Gailloud P, Beauchamp NJ et al (2002) Is percutaneous vertebroplasty without pretreatment venography safe? Evaluation of 205 consecutives procedures. Am J Neuroradiol 23:913–917
6. Peh WC, Gilula LA (2003) Additional value of a modified method of intraosseous venography during percutaneous vertebroplasty. AJR 180:87–91
7. Leibold RA, Gilula LA (2002) Sterilization of barium for vertebroplasty: an effective, reliable, and inexpensive method to sterilize powders for surgical procedures. AJR 179:198–200
8. Groen RJ, du Toit DF, Phillips FM et al (2004) Anatomical and pathological considerations in percutaneous vertebroplasty and kyphoplasty: a reappraisal of the vertebral venous system. Spine 29:1465–1471
9. Baston OV (1940) The function of the vertebral veins and their role in the spread of metastases. Arch Surg 112:138–149
10. Hawkins IF, Caridi JG (1998) Carbon dioxide (CO2) digital subtraction angiography: 26-year experience at the University of Florida. Eur Radiol 8:391–402
11. Chung SE, Lee SH, Kim TH et al (2006) Renal cement embolism during percutaneous vertebroplasty. Eur Spine J Suppl 5:590–594

Corpus Callosum in Patients with Obsessive-Compulsive Disorder: Diffusion-Tensor Imaging Study[1]

Yukiko Saito, MD
Kenji Nobuhara, MD, PhD
Gaku Okugawa, MD, PhD
Katsunori Takase, MD, PhD
Tatsuya Sugimoto, MD
Mami Horiuchi, MD
Chiho Ueno, MD
Minoru Maehara, MD
Naoto Omura, MD
Hiroaki Kurokawa, MD, PhD
Koshi Ikeda, MD, PhD
Noboru Tanigawa, MD, PhD
Satoshi Sawada, MD, PhD
Toshihiko Kinoshita, MD, PhD

Purpose: To prospectively examine microstructural white matter abnormalities in the corpus callosum (CC) of patients with obsessive-compulsive disorder (OCD), as compared with control subjects, and to investigate the relationship between diffusion-tensor (DT) imaging measures of the CC region and clinical symptoms of OCD.

Materials and Methods: Institutional review board approval was obtained, and each participant—or the participant's parent(s)—provided written informed consent. Sixteen patients with OCD (seven male, nine female; mean age, 28.7 years ± 9.8 [standard deviation]) and 16 matched healthy volunteers (control subjects) (seven male, nine female; mean age, 29.9 years ± 9.0) were examined. Mean diffusivity and fractional anisotropy (FA) were measured in five subdivisions of the CC. The paired *t* test was performed to compare the mean diffusivity or the FA in CC regions between the patients with OCD and the control subjects.

Results: There were no significant differences (rostrum, $P = .15$; genu, $P = .88$; rostral body, $P = .12$; isthmus, $P = .77$; splenium, $P = .88$) in mean diffusivity between the patients with OCD and the healthy volunteers. A significant reduction in FA was observed in the rostrum of the CC in patients with OCD compared with the rostral FA in the control subjects ($P < .001$). Higher FA in only the rostrum correlated significantly with lower Yale-Brown obsessive-compulsive scale score ($r = -0.72$, $P = .002$).

Conclusion: Study results support the widely held view that the orbital prefrontal region is involved in the pathophysiology of OCD and indicate that the orbitofrontal circuit influences symptom severity in patients with OCD.

[1] From the Departments of Neuropsychiatry (Y.S., K.N., G.O., K.T., T.S., M.H., C.U., T.K.) and Radiology (Y.S., M.M., N.O., H.K., K.I., N.T., S.S.), Kansai Medical University, 10-15 Fumizono-cho, Moriguchi City, Osaka, 570-8506, Japan. Received August 23, 2006; revision requested October 30; revision received March 2, 2007; accepted March 21; final version accepted July 5. Supported by grant 16591173 from the Ministry of Education Science and Culture of Japan. Address correspondence to Y.S. (e-mail: *saitoyu@takii.kmu.ac.jp*).

Obsessive-compulsive disorder (OCD) is characterized by intense, intrusive, and unwanted thoughts or ideas in association with urges to perform ritualistic behaviors (1). OCD is often chronically disabling, with concomitant impairments in interpersonal and occupational function, and patients with this disorder report having senseless and unpleasant symptoms (2). Obsessions and compulsions typically emerge around the 2nd to 3rd decade of life and often are resistant to psychodynamic therapeutic approaches; however, they are quite responsive to pharmacologic intervention (3).

Neuropsychologic studies have revealed cognitive impairments with OCD (4,5). The corpus callosum (CC), the largest interhemispheric white matter commissure connecting the cerebral hemispheres, has a crucial role in interhemispheric communication and cognitive processes (6). The subdivisions of the CC may be roughly associated with various cortical regions, although there is considerable overlap. The possibility of topographic organization of callosal fibers is based on experimental work with monkeys (7), autoradiographic study results (8,9), and clinical study results (10,11). The rostrum contains fibers from the orbitofrontal cortex (OFC), and the genu connects the lateral and medial surfaces of the frontal lobes. The body of the CC connects wide neocortical homotopic regions of the cerebral hemispheres, including the premotor, supplementary motor, motor, somatesthetic, and posterior parietal regions. The isthmus connects the superior temporal and posterior parietal regions, while the splenium connects the occipital and inferior temporal regions.

Neuroimaging study results have repeatedly implicated the OFC in the pathophysiology of OCD. The OFC, when measured at baseline (12,13) or during exposure (14) to triggering stimuli, is hyperactive in patients with OCD. Substantial reductions in OFC activity have been observed after successful pharmacologic and behavioral therapy (15). The consistency with which OFC hyperactivity has been observed in these studies suggests that the OFC may make a unique contribution to OCD. The OFC is positioned at a point of interface between the sensory association cortices, limbic structures, and subcortical regions involved in controlling the automatic and motor effector pathways (16). Although recent research on OCD has been focused on the neuroanatomic circuitry, including the circuitry in the OFC, the abnormalities of the white matter in the orbitofrontal region in patients with OCD have been examined in only a few studies.

Magnetic resonance (MR) diffusion-tensor (DT) imaging is used to noninvasively examine the molecular diffusion of water in vivo and to directly appreciate the anatomic integrity of neural fibers (axons and myelin) in white matter. Thus, DT imaging yields information about white matter tracts and their organization (17). Specifically, it yields an index of microstructural integrity through quantification of the magnitude and directionality of restricted tissue water mobility (diffusion anisotropy) in three dimensions. The magnitude and directionality are evaluated specifically by using measurements of mean diffusivity (D_M), a measure of the magnitude of diffusion, and fractional anisotropy (FA), a measure of the directionality of diffusion. DT imaging has been used successfully to evaluate the white matter fiber integrity in patients with psychiatric diseases such as schizophrenia (18–20) and depression (21).

We hypothesized that OCD is associated with white matter integrity abnormalities in the orbitofrontal brain region. Thus, the purpose of our study was to prospectively examine the microstructural white matter abnormalities in the CC of patients with OCD, as compared with healthy control subjects, and to investigate the relationship between DT measures of the CC region and clinical symptoms of OCD.

Advance in Knowledge

- In patients with obsessive-compulsive disorder (OCD), we observed abnormal white matter anisotropy in the rostrum of the corpus callosum (CC) and an inverse relationship between white matter anisotropy in the CC rostrum and severity of OCD symptoms.

Implication for Patient Care

- Diffusion-tensor imaging performed in addition to Yale-Brown obsessive-compulsive scale scoring may help to predict the severity of OCD symptoms.

Materials and Methods

Patients

The study protocol was approved by our institutional review board, and written informed consent was obtained from all patients or their parents, depending on the age of the patient. All patients had received a diagnosis of OCD based on criteria listed in the fourth edition of the *Diagnostic and Statistical Manual of Mental Disorders* (DSM-IV) (22). Between April 2004 and October 2005, 18 consecutive patients with OCD who met

Published online before print
10.1148/radiol.2462061469

Radiology 2008; 246:536–542

Abbreviations:
CC = corpus callosum
D_M = mean diffusivity
DT = diffusion tensor
FA = fractional anisotropy
HDRS = Hamilton Depression Rating Scale
OCD = obsessive-compulsive disorder
OFC = orbitofrontal cortex
ROI = region of interest
STIR = short inversion time inversion recovery
Y-BOCS = Yale-Brown Obsessive-Compulsive Scale

Author contributions:
Guarantors of integrity of entire study, Y.S., K.N.; study concepts/study design or data acquisition or data analysis/interpretation, all authors; manuscript drafting or manuscript revision for important intellectual content, all authors; manuscript final version approval, all authors; literature research, Y.S., K.N., G.O., H.K., K.I.; clinical studies, Y.S., K.N., G.O., K.T., T.S., C.U., H.K., K.I.; statistical analysis, Y.S., K.N., G.O.; and manuscript editing, all authors

Authors stated no financial relationship to disclose.

our study criteria were recruited for this investigation at our university hospital. We excluded patients who *(a)* had cardiac pacemakers, metallic clips, or other metallic implants or artifacts in their bodies; *(b)* had substantial medical illness or neurologic (eg, Tourette syndrome, Huntington disease, and Parkinson disease), pulmonary, cardiac, renal, hepatic, endocrine, or metabolic disorders; *(d)* had DSM-IV-defined dementia, delirium, schizophrenia, schizoaffective disorder, delusional disorder, brief reactive psychosis, or psychotic disorders not otherwise specified; *(e)* had DSM-IV-defined mental retardation; *(f)* had lacunar infarcts; *(g)* were currently or previously dependent on or abusers of DSM-IV-defined alcoholic or psychoactive substances; and/or *(h)* were pregnant. All patients with lacunar infarcts in any location were excluded. Thus, two patients found to have lacunar infarction were excluded from our study. The final study cohort included 16 patients (seven male, nine female; age range, 16–47 years; mean age, 28.7 years ± 9.8 [standard deviation]).

The final study cohort of 16 patients had a mean total Yale-Brown Obsessive-Compulsive Scale (Y-BOCS) score of 26.0 ± 5.3, and their mean scores on the obsessive and compulsive subscales were 14.6 ± 3.5 and 11.4 ± 2.8, respectively. Their mean Hamilton Depression Rating Scale (HDRS) score was 5.3 ± 2.7. No patients had comorbid disorders such as major depression or panic disorder. Ten patients had doubting obsessions (wondering whether something was done) in association with checking compulsions (checking that it was done), whereas six patients had contamination obsessions (fear of germs) in association with washing compulsions.

All but three patients were receiving medication for their OCD symptoms at the time of the MR examination: Five patients were taking paroxetine hydrochloride only; two patients, a combination of paroxetine hydrochloride and benzodiazepines; and two patients, a combination of fluvoxamine maleate and benzodiazepines. One patient each was taking a combination of paroxetine hydrochloride, fluvoxamine maleate, and benzodiazepines; a combination of paroxetine hydrochloride and clomipramine hydrochloride; a combination of fluvoxamine maleate, benzodiazepines, and sulpiride; or a combination of fluvoxamine maleate, milnacipran hydrochloride, and benzodiazepines.

Control Subjects

Sixteen healthy volunteers (seven male, nine female; age range, 16–47 years; mean age, 29.9 years ± 9.0) matched one-to-one in age, sex, and handedness with the patients who had OCD participated in the study as control subjects after giving informed consent. Institutional review board approval was also obtained to examine these volunteers. Neither these volunteers nor their first-degree relatives had a history of psychiatric illness. They underwent MR imaging of the brain and were subsequently confirmed to have normal MR findings and no neurologic deficits at clinical examination.

Clinical Assessments

Only the 16 patients with OCD were examined with the Y-BOCS and the 17-item HDRS. Greater symptom severity results in higher Y-BOCS and HDRS scores. Both assessments were performed by one trained psychiatrist (Y.S., 5 years experience in psychiatry) at the initial visit, 2 weeks before the MR examinations.

MR Imaging Protocol

The MR examinations were performed with a 1.5-T unit (Signa Horizon LX; GE Medical Systems, Milwaukee, Wis). Head motion was minimized with restraining pads and tape before imaging. Echo-planar MR images were obtained in the patients with OCD and the control subjects and were checked for head motion. Sagittal short inversion time inversion-recovery (STIR) echo-planar images were acquired first, with a section clearly showing the anterior and posterior commissures. The superoinferior thickness of the rostrum in the sagittal plane was measured. Then, a series of transverse diffusion-weighted images with a diffusion-sensitizing gradient (b = 1000 sec/mm^2) were obtained. Diffusion was measured along six noncolinear directions. We used single-shot spin-echo echo-planar sequences for DT analysis. All acquisitions were performed parallel to the anterior commissure–posterior commissure line with use of the following parameters: >17 000/>115.6 (repetition time msec/echo time msec), 128 × 128 matrix, 24 × 24-cm field of view, four signals acquired, 4.0-mm section thickness, and no intersection gap.

The diffusion-weighted images were transferred to a dedicated workstation (Sun Microsystems, Santa Clara, Calif), where the DT data were postprocessed by using Functool 2.2.49 software (GE Medical Systems). Echo-planar image distortion was corrected. The first step of this procedure entails correcting the distortions usually induced by the eddy current related to the large diffusion-sensitizing gradients. This correction algorithm is based on the maximization of mutual information to estimate the three parameters of a geometric distortion model inferred from the acquisition principle. The second step of the procedure involves replacing the standard least squares–based approach with the Geman-McLure M estimator approach to eliminate outlier-related artifacts.

D_M and FA maps were then computed by using the DT data. The Functool software applies thresholding to apparent diffusion coefficient maps that may substantially affect mean region-of-interest (ROI) data. We were aware of this and took care to avoid it.

Diffusion eigenvectors and eigenvalues (λ_1, λ_2, and λ_3), which correspond to the main diffusion direction and the associated diffusivity, were calculated from the DT data. FA values, which yield information about the degree of diffusion anisotropy in white matter, and D_M values, which yield information about the magnitude of diffusion, were then calculated:

$$FA = \sqrt{\frac{3}{2}} \cdot \frac{\sqrt{(\lambda_1 - \lambda)^2 + (\lambda_2 - \lambda)^2 + (\lambda_3 - \lambda)^2}}{\sqrt{\lambda_1^2 + \lambda_2^2 + \lambda_3^2}}$$

and

$$D_M = (\lambda_1 + \lambda_2 + \lambda_3)/3.$$

ROI Selection and Analysis

The CC was clearly delineated in the midsagittal plane on the STIR brain MR images. The lack of anatomic landmarks on the midsagittal view of the CC made it difficult to define the corresponding cortical areas from which the fibers originate. Thus, seven callosal subdivisions were defined on the basis of the scheme of regional divisions of the CC proposed by Witelson and Kigar (23) (Fig 1a). We investigated the plane parallel to the anterior commissure–posterior commissure plane, including each subdivision of the CC, on the sagittal STIR images (Fig 1b). Each ROI consisted of manually traced 2-mm squares placed over the anatomic horizontal T2-weighted imaging plane, which was determined on the basis of the sagittal STIR image findings. The borderlines between the anterior middle and posterior middle bodies of the CC were not clearly defined in the transverse T2-weighted imaging planes. Therefore, the following five subdivisions of the CC were chosen as ROIs: the rostrum, genu, rostral body, isthmus, and splenium (Fig 2).

Two trained physicians (Y.S., K.N.) conducted all FA measurements in consensus. These physicians have 5 (Y.S.) and 10 (K.N.) years experience in brain MR imaging research. They were blinded to the subject group when they performed the ROI analysis. For each subject, the ROIs were transferred onto FA maps and the FA was calculated for each selected CC ROI. The interoperator reliability between the two physicians in assessing the DT measures in 10 randomly selected subjects (five patients with OCD, five healthy volunteers) was also confirmed.

Statistical Analyses

The two physicians (Y.S., K.N.) were blinded to information about the images that they were analyzing. Interoperator reliability in assessing the DT measures was confirmed by using intraclass correlation coefficients. Data for 10 participants (five patients with OCD, five healthy volunteers) collected by one psychiatrist (K.N.) were used to compare the patient and control subject data. Mean DT values for each ROI, including 95% confidence intervals for the difference in mean values between

Figure 1

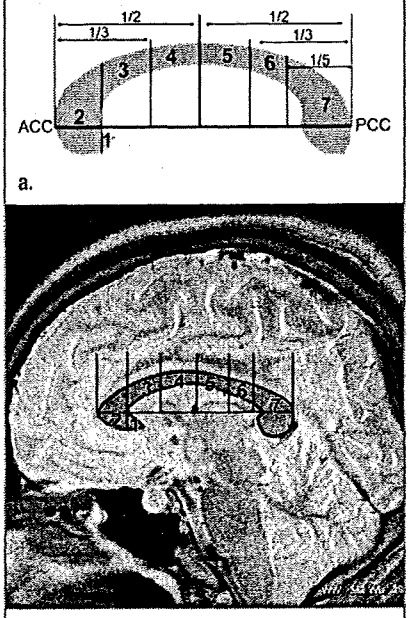

Figure 1: Regional subdivisions of CC in adult human based on **(a)** regional division scheme of the CC and **(b)** corresponding sagittal STIR MR image findings (3000/8.8/100 [repetition time msec/echo time msec/inversion time msec]). Anterior CC *(ACC)* and posterior CC *(PCC)* are extreme anterior and extreme posterior points of the CC, respectively, with anterior CC–posterior CC distance defined as the length of the CC. Anterior CC–posterior CC distance is used as linear axis to subdivide CC into anterior and posterior halves; anterior, middle, and posterior thirds; and posterior fifth region, which is roughly congruent with the splenium (region *7*). Line perpendicular to axis at extreme anterior point on inner convexity of anterior CC is used to define rostrum (region *1*) and extreme anterior division of CC, which is roughly congruent with the genu (region *2*). Region *3*, the rostral body, is defined as anterior third of CC minus regions *1* and *2*. Region *4*, the anterior middle body, is defined as anterior half minus anterior third. Region *5*, the posterior middle body, is defined as posterior half minus posterior third. Region *6*, the isthmus, is defined as posterior third minus posterior fifth. Regions *3–6* constitute CC body.

Figure 2

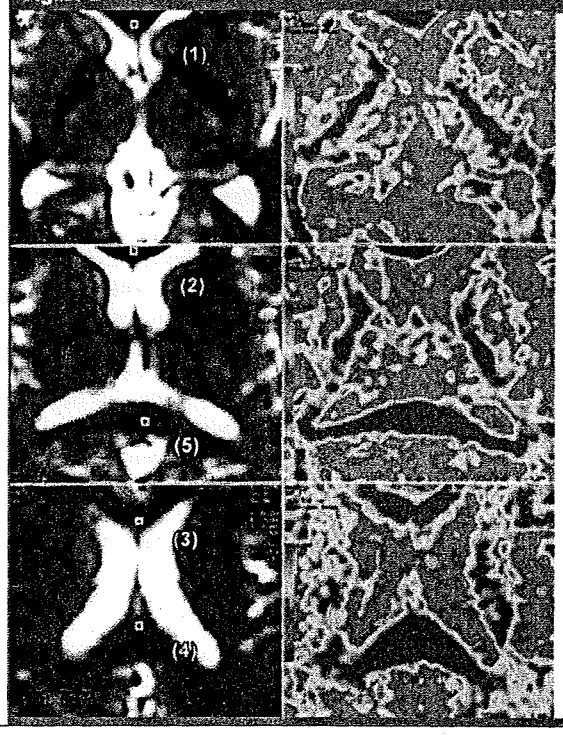

Figure 2: Transverse T2-weighted MR images (left, $b = 0$ sec/mm^2) and corresponding FA maps (right, $b = 1000$ sec/mm^2) in patient with OCD (>17 000/>115.6, 4-mm section thickness). ROIs are drawn in rostrum *(1)*, genu *(2)*, rostral body *(3)*, isthmus *(4)*, and splenium *(5)* of CC. Right: Colors, demonstrated by using Functool 2.2.49 software, indicate various grades of white matter anisotropy. Blue indicates low grade of white matter anisotropy, and red indicates high grade of white matter anisotropy.